

A DFT/TD-DFT study of effect of different substituent on ESIPT fluorescence features of 2-(2'-hydroxyphenyl)-4-chloromethylthiazole derivatives

Shen-Yang Su(苏申阳), Xiu-Ning Liang(梁秀宁), and Hua Fang(方华)

Citation: Chin. Phys. B, 2022, 31 (**3**): 038202. DOI: 10.1088/1674-1056/ac21c6
Journal homepage: http://cpb.iphy.ac.cn; http://iopscience.iop.org/cpb

What follows is a list of articles you may be interested in

Relationship between ESIPT properties and antioxidant activities of 5-hydroxyflavone derivates

Chaofan Sun(孙朝范), Bifa Cao(曹必发), Hang Yin(尹航), Ying Shi(石英)
Chin. Phys. B, 2020, 29 (**5**): 058202. DOI: 10.1088/1674-1056/ab7ea1

Theoretical study on the relationship between the position of the substituent and the ESIPT fluorescence characteristic of HPIP

Xin Zhang(张馨), Jian-Hui Han(韩建慧), You Li(李尤), Chao-Fan Sun(孙朝范), Xing Su(苏醒), Ying Shi(石英), Hang Yin(尹航)
Chin. Phys. B, 2020, 29 (**3**): 038201. DOI: 10.1088/1674-1056/ab6d50

Effect of intramolecular and intermolecular hydrogen bonding on the ESIPT process in DEAHB molecule

Hui Li(李慧), Lina Ma(马丽娜), Hang Yin(尹航), Ying Shi(石英)
Chin. Phys. B, 2018, 27 (**9**): 098201. DOI: 10.1088/1674-1056/27/9/098201

Improved electrochemical performances of high voltage $LiCoO_2$ with tungsten doping

Jie-Nan Zhang(张杰男), Qing-Hao Li(李庆浩), Quan Li(李泉), Xi-Qian Yu(禹习谦), Hong Li(李泓)
Chin. Phys. B, 2018, 27 (**8**): 088202. DOI: 10.1088/1674-1056/27/8/088202

Crystal structure and ionic conductivity of Mg-doped apatite-type lanthanum silicates $La_{10}Si_{6-x}Mg_xO_{27-x}$($x$=0-0.4

Yin Guang-Chao, Yin Hong, Zhong Lin-Hong, Sun Mei-Ling, Zhang Jun-Kai, Xie Xiao-Jun, Cong Ri-Dong, Wang Xin, Gao Wei, Cui Qi-Liang
Chin. Phys. B, 2014, 23 (**4**): 048202. DOI: 10.1088/1674-1056/23/4/048202

A DFT/TD-DFT study of effect of different substituent on ESIPT fluorescence features of 2-(2′-hydroxyphenyl)-4-chloro-methylthiazole derivatives

Shen-Yang Su(苏申阳)†, Xiu-Ning Liang(梁秀宁), and Hua Fang(方华)

Department of Chemistry and Material Science, College of Science, Nanjing Forestry University, Nanjing 210037, *China*

(Received 15 May 2021; revised manuscript received 15 May 2021; accepted manuscript online 27 August 2021)

Based on density functional theory (DFT) and time-dependent density functional theory (TD-DFT), the effects of substituent on the excited-state intramolecular proton transfer (ESIPT) process and photophysical properties of 2-(2′-hydroxyphenyl)-4-chloromethylthiazole (HCT) are studied. The electron-donating group (CH_3, OH) and electron-withdrawing group (CF_3, CHO) are introduced to analyze the changes of intramolecular H-bond, the frontier molecular orbitals, the absorption/fluorescence spectra, and the energy barrier of ESIPT process. The calculation results indicate that electron-donating group strengthens the intramolecular H-bond in the S_1 state, and leads to an easier ESIPT process. The electron-withdrawing group weakens the corresponding H-bond and makes ESIPT process a little harder. Different substituents also affect the photophysical properties of HCT. The electron-withdrawing group (CF_3, CHO) has a little effect on electronic spectra. The electron-donating group (CH_3, OH) red-shifts both the absorption and fluorescence emission peaks of HCT, respectively, which causes the Stokes shift to increase.

Keywords: excited-state intramolecular proton transfer (ESIPT), TD-DFT, substitution

PACS: 82.39.Jn, 31.15.ee, 87.15.ht **DOI:** 10.1088/1674-1056/ac21c6

1. Introduction

As a typical weak interaction, hydrogen bond (H-bond) plays a significant part in biology, chemistry, and physics, especially in many photochemical and photophysical processes.[1–6] Proton transfer (PT) usually occurs in molecules with acidic and basic groups, and the H-bond between the acidic group and basic group i acts as the bridge of proton transfer. Since the excited state proton transfer process was reported first by Weller,[7] a strong upsurge to study the excited state intramolecular and intermolecular proton transfer has sustained for decades.

Excited-state intramoecular proton transfer (ESIPT) reaction is a sub-picosecond ultrafast photo-induced tautomerization process, in which the ground-state normal form (N) converts into the corresponding tautomer form (T) by undergoing a four-stage photocycle.[8–10] The transformation between N and T results in great changes in the physical and chemical properties of the compound, especially in the spectral behaviors. In the photocycle process, dual fluorescent emission and large Stokes shift are observed in ESIPT compound. Based on the unique photophysical features, ESIPT molecules are widely applied to photostabilizer, sensing technology, molecular switches, and laser dyes.[11–17]

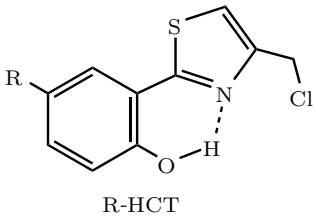
The fluorescent properties of ESIPT compound are obviously affected by the media environment, such as pH, solvent polarity, solvent type, viscosity, *etc*. Many researchers have performed a large number of studies on the effects of surrounding media on ESIPT process and luminescent properties.[18–22] In addition, the changes of geometrical structures of ESIPT compound can also control the spectral features. The substitution of functional groups may provide an effective way to fine-tune the ESIPT process and photophysical properties of compounds.[23–26] According to the previous reports, Ma *et al.*[27] studied the substituent effect on ESIPT process of 1-(aclamino)-anhraquinones. Takagi *et al.*[28] probed the ESIPT fluorescence properties of methoxy-substituted 2-hydroxyphenylbenzimidazole. Song *et al.*[29] investigated the effect of different substiuents on ESIPT of 3-hydroxychromone. Zhang *et al.*[30] examined the relationship between the substituted position and ESIPT fluorescence features of 2-(2′-hydroxyphenyl)imidazo[1,2-*a*]-pyridine (HPIP). Zhang *et al.*[31] synthesized a series of new NH-type pyrroleindole compounds and discussed the effects of different functional groups on the ESIPT process and photophysical properties. Obviously, an approporiate substituent can greatly improve the properties of ESIPT materials. Therefore, structural modification with different functional groups can usually be used to design and develop new ESIPT compounds with good applications.

Recently, a series of thiazole-based organic molecules[32–37] was synthesized experimentally and successfully used as fluorescent chemosensors with high selectivity in identifying metal ions (*e.g.*, Ga^{3+}, Al^{3+}, Zn^{2+}, Cu^{2+}) and anions (*e.g.*, CN^-, F^-, I^-, HSO_4^-, $H_2P_2O_7^{3-}$). The diversities of fluorescence recognition functions of the parent thi-

†Corresponding author. E-mail: susanfang20@gmail.com

© 2022 Chinese Physical Society and IOP Publishing Ltd

azole molecule are due to the chemical modification in the positions 2 and 4 of the thiazole ring. Inspired by the previous reports, we investigate the effects of different substituents on the ESIPT process and photophysical properties of fluorescent probe molecule in the present work. We design four novel ESIPT compounds via chemical substitution based on 2-(2′-hydroxyphenyl)-4-chloromethylthiazole (HCT).[33] Two electron-donating groups (CH_3, OH) and two electron-withdrawing groups (CF_3, CHO) are introduced in the para position of hydroxyl group in the benzene ring of HCT, and denoted as R-HCT. The structures of the designed probes R-HCT are shown in Fig. 1. We employ the density functional theory (DFT) and time-dependent DFT (TD-DFT) to investigate the effects of different substituents on the intramolecular H-bond, the absorption/fluorescence spectra and ESIPT process of R-HCT. Detailed calculation results, such as structural parameter, vibrational spectra, topology analysis, reduced density gradient analysis, frontier molecular orbital, ESIPT process, and photophysical properties are investigated as follows. We hope our studies may provide much useful information for the design of ESIPT-based fluorescent probes with better photophysical properties.



R-HCT

R	R-HCT
H	HCT
CH_3	CH_3-HCT
OH	OH-HCT
CF_3	CF_3-HCT
CHO	CHO-HCT

Fig. 1. Structures of R-HCT (R: H, CH_3, OH, CF_3, CHO).

2. Computational details

In this work, all the calculations were performed by using the Gaussian 09 package.[38] The ground-state (S_0) and the first excitedstate (S_1) normal form (N), transition state (TS), and tautomer form (T) of R-HCT (R: CH_3, OH, CF_3, CHO) molecules were fully optimized by using the DFT and TD-DFT methods with B3PW91 functional[39–41] and 6-31+G(d, p) basis set. The frequency calculations were carried out at the same computational level to verify the minima (N and T) and transition state, which have no imaginary frequency and only one imaginary frequency, respectively. Acetonitrile solvent and the integral equation polarizable continuum model (IEFPCM)[42–44] were chosen in order to be consistent with the experimental environment.[33] The absorption and fluorescence emission spectra were simulated at a TD-B3PW91/6-31+G(d,p) level based on the optimized S_0 structure and optimized S_1 structure, respectively. The topology analysis and the reduced density gradient isosurfaces were performed by using the Multiwfn program[45] and VMD program,[46] respectively.

3. Results and discussion

3.1. Optimized structures and infrared spectra

All the structures of HCT derivatives R-HCT (R: CH_3, OH, CF_3, CHO) in the normal (N) and tautomer (T) forms in the S_0 and S_1 states are completely optimized and shown in Fig. 2. The corresponding structural parameters related to intramolecular H-bond in R-HCT, such as bond lengths O_1–H_2, H_2–N_3, and bond angle O_1–H_2–N_3, are listed in Table 1.

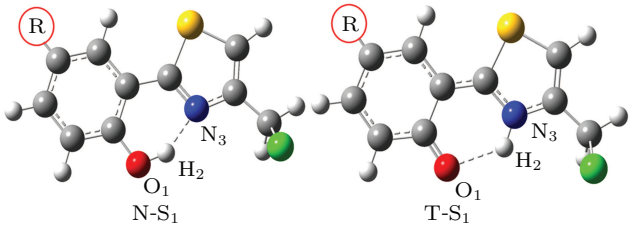


Fig. 2. Optimized geometries of normal form (N) and tautomer form (T) of R-HCT (R: CH_3, OH, CF_3, CHO) in S_1 state.

For the normal forms of CH_3-HCT and OH-HCT compound, it can be seen in Table 1 that the bond distances of O_1–H_2 and H_2–N_3, and the bond angle O_1–H_2–N_3 in the S_0 state are 0.996 Å, 1.703 Å, 147.9°, and 0.995 Å, 1.709 Å, 147.8° respectively. Comparing with HCT,[47] the H_2–N_3 bonds and the angles O_1–H_2–N_3 of CH_3-HCT and OH-HCT in the S_0 state are elongated and shortened, respectively, which means that the intramolecular H-bonds O_1–H_2…N_3 of CH_3-HCT and OH-HCT in the S_0 state are weaker than those of HCT. The electron-donating groups CH_3 and OH evidently weaken the intramolecular H-bond of HCT in the S_0 state. For the CHO-HCT compound and CF_3-HCT compound, the H_2–N_3 bond distances and the bond angles O_1–H_2–N_3 averagely decrease by 0.024 Å and increase by 0.15°, respectively, compared with the corresponding data of HCT. The shortened H_2–N_3 bond and the enlarged O_1–H_2–N_3 angle confirm the existence of the strong intramolecular H-bond O_1–H_2…N_3 in CF_3-HCT and CHO-HCT compounds in the S_0 state. However, the effects of different functional groups (CH_3, OH, CF_3, CHO) on the structure of HCT in the S_1 state are quite opposite. From Table 1 it follows that the bond distance of H_2–N_3 and bond angle of O_1–H_2–N_3 for each of CH_3-HCT and OH-HCT are averagely shortened by 0.059 Å and enlarged by 1.1°, respectively, and the corresponding parameters of R-HCT (R: CF_3, CHO) are averagely elongated by 0.022 Å and reduced by 0.9°, respectively, compared with those of HCT. These results indicate that the intramolecular H-bond of HCT in the S_1 state is enhanced by the electron-donating group (CH_3, OH) and weakened by the electron-withdrawing group (CF_3, CHO). In addition, the O_1–H_2 and H_2–N_3 bond lengths and O_1–H_2–N_3 bond angle of R-HCT (R: CH_3, OH, CF_3, CHO) are in a range of 0.995 Å–1.003 Å, 1.670 Å–1.709 Å, and 147.8°–148.4° in the S_0 state, and in a range of 1.023 Å–1.057 Å,

1.508 Å–1.610 Å, and 150.7°–152.9° in the S_1 state, respectively. The elongating O_1–H_2 bond, the shortening H_2–N_3 bond, and the enlarging O_1–H_2–N_3 bond angle of the R-HCT (R: CH_3, OH, CF_3, CHO) confirm that the intramolecular H-bond O_1–H_2…N_3 are strengthened in the S_1 state, which will be favorable to occur in the ESIPT process.

For the R-HCT (R: CH_3, OH, CF_3, CHO) compounds, the tautomer forms cannot be obtained in the S_0 state. Each attempt to find the tautomer structures fails. These results suggest that the R-HCT compounds radioatively return to the ground state in the tautomer form, subsequently return to the normal forms in a barrierless manner.

Table 1. Primary structural parameters (bond length (in unit Å) and bond angle in unit (°)) of HCT and its derivatives R-HCT (R: CH_3, OH, CF_3, CHO) in S_0 state and S_1 state.

System	Form	S_0			S_1		
		O_1–H_2	H_2–N_3	O_1–H_2–N_3	O_1–H_2	H_2–N_3	O_1–H_2–N_3
HCT[47]	N	0.997	1.700	148.1	1.033	1.575	151.8
	T				1.868	1.029	130.5
CH_3-HCT	N	0.996	1.703	147.9	1.057	1.508	152.9
	T				1.825	1.031	132.7
OH-HCT	N	0.995	1.709	147.8	1.049	1.525	152.8
	T				1.782	1.036	134.5
CF_3-HCT	N	1.001	1.682	148.1	1.023	1.610	150.7
	T				1.896	1.025	129.1
CHO-HCT	N	1.003	1.670	148.4	1.030	1.583	151.2
	T				1.905	1.023	128.6

The changing of intramolecular H-bond of R-HCT (R: CH_3, OH, CF_3, CHO) can be confirmed by the infrared (IR) vibration spectra of the O_1–H_2 bond (normal form) in the R-HCT compounds in acetonitrile (shown in Fig. 3). In general, the strengthening or weakening of H-bond corresponds to the red-shift or blue-shift of O_1–H_2 bond stretching vibrational frequency, respectively.[48–50] As shown in Fig. 3, the O_1–H_2 stretching vibrational frequencies for CH_3-HCT, OH-HCT, CF_3-HCT, and CHO-HCT in the S_0 state are at 3189 cm^{-1}, 3215 cm^{-1}, 3110 cm^{-1}, and 3063 cm^{-1}, respectively. When R-HCT (R: CH_3, OH, CF_3, CHO) compounds are in the S_1 state, the corresponding vibrational frequencies are situated on 2153 cm^{-1}, 2266 cm^{-1}, 2680 cm^{-1}, and 2551 cm^{-1}, respectively. The O_1–H_2 stretching vibrational frequencies of HCT replaced by electron-donating group and electron-withdrawing group are slightly blue-shifted and red-shifted in the S_0 state, respectively, in comparison with the corresponding value of HCT.[47] These results confirm the electron-donating group (CH_3 and OH) and electron-withdrawing group (CF_3, CHO) weaken and strengthen the intramolecular H-bond O_1–H_2…N_3 in the S_0 state, respectively. In the S_1 state, the substituents have opposite effects on the intramolecular H-bond based on the changes between HCT and R-HCT (R: CH_3, OH, CHO, CF_3). In addition, the apparent red-shifts 1036 cm^{-1}, 949 cm^{-1}, 430 cm^{-1}, and 512 cm^{-1} of the O_1–H_2 stretching vibrational frequency of CH_3-HCT, OH-HCT, CF_3-HCT, and CHO-HCT in the S_1 state, respectively, represent the strengthening intramolecular H-bond O_1–H_2… N_3, compared with the corresponding IR frequencies in the S_0 state. The proton might transfer more easily in the S_1 state than in the S_0 state. The red-shift values between S_0 and S_1 states in CH_3-HCT and OH-HCT are larger than those values in R-HCT (R: CHO, CF_3), which means that the electron-donating group has stronger effects on enhancing the intramolecular H-bond than electron-withdrawing group. The conclusion obtained by the structural parameters is proved by the analysis of IR vibration.

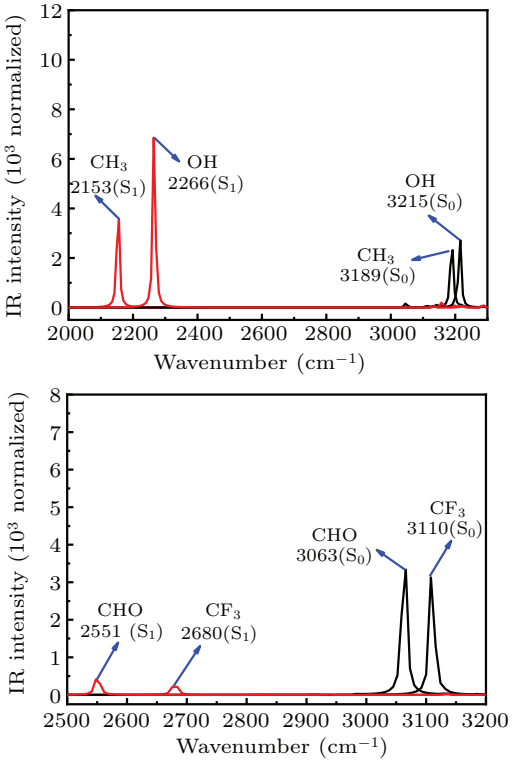


Fig. 3. IR spectra for R-HCT (R: CH_3, OH, CF_3, CHO) in the normal form in a region of O_1–H_2 stretching vibration spectra in S_0 state and S_1 state.

3.2. Topology analysis and reduced density gradient analysis

To further explore the strength of intramolecular H-bond of R-HCT (R: CH_3, OH, CF_3, CHO), the topological analysis based on the electron density is performed. Topology parameters ($\rho(r)$, $\nabla^2\rho(r)$, $V(r)$, E_{HB}, $G(r)$, $H(r)$, and ELF) are obtained at the bond critical point (BCP, [3,-1] type) between H_2 atom and N_3 atom and listed in Table 2. The value of $\nabla^2\rho(r)$ can be used to determine the type of interaction, and the value of $\rho(r)$ and E_{HB} are closely related to the strength of the H-bond.[51] The positive or negative value of $\nabla^2\rho(r)$ represents the closed-shell interaction (*e.g.*, ionic bond and H-bond) or shared interaction (*e.g.*, covalent bond), respectively. The H-bond strength can be divided into three types based on the value of $\rho(r)$ at BCP:[52] (i) weak, $\rho(r) \leq 0.02$; (ii) medium, $0.02 < \rho(r) < 0.03$; (iii) strong, $\rho(r) \geq 0.03$. The bigger the values of $\rho(r)$ and E_{HB} are, the stronger the H-bond is. It can be found in Table 2 that the electron density $\rho(r)$ of R-HCT (R: CH_3, OH, CF_3, CHO) in the S_0 and S_1 states are in a range of 0.0512 a.u.–0.0547 a.u. and 0.0648 a.u.–0.0845 a.u., respectively, and the value of Laplacian $\nabla^2\rho(r)$ in the S_0 state and the S_1 state are larger than 0.10 a.u.

Table 2. Calculated BCP parameters associated with intramolecular H-bond of R-HCT (R: CH_3, OH, CF_3, CHO) in S_0 state and S_1 state.

Compound	$\rho(r)$[a]	$G(r)$[b]	$V(r)$[c]	$H(r)$[d]	E_{HB}[e]	$\nabla^2\rho(r)$[f]
HCT-S_0[47]	0.0522	0.0355	–0.0407	–0.0051	–10.9025	0.1217
CH_3HCT-S_0	0.0519	0.0354	–0.0403	–0.0050	–10.8316	0.1215
OH-HCT-S_0	0.0512	0.0350	–0.0397	–0.0047	–10.6745	0.1211
CF_3HCT-S_0	0.0547	0.0370	–0.0432	–0.0062	–11.4676	0.1233
CHO-HCT-S_0	0.0537	0.0380	–0.0450	–0.0070	–11.2453	0.1238
HCT-S_1[47]	0.0708	0.0469	–0.0631	–0.0162	–15.0518	0.1229
CH_3HCT-S_1	0.0845	0.0544	–0.0831	–0.0287	–18.1031	0.1030
OH-HCT-S_1	0.0806	0.0526	–0.0773	–0.0247	–17.2395	0.1116
CF_3HCT-S_1	0.0648	0.0432	–0.0550	–0.0118	–13.7132	0.1253
CHO-HCT-S_1	0.0695	0.0459	–0.0611	–0.0152	–14.7603	0.1226

[a] $\rho(r)$ is electron density (in unit a.u.). [b] $G(r)$ is kinetic energy density (in unit a.u.).
[c] $V(r)$ is potential energy density (in unit a.u.). [d] $H(r)$ is total electron energy density (in unit a.u.).
[e] E_{HB} is hydrogen bond energy (in unit kcal/mol). [f] $\nabla^2\rho(r)$ is Laplacian of electron density (in unit a.u.).

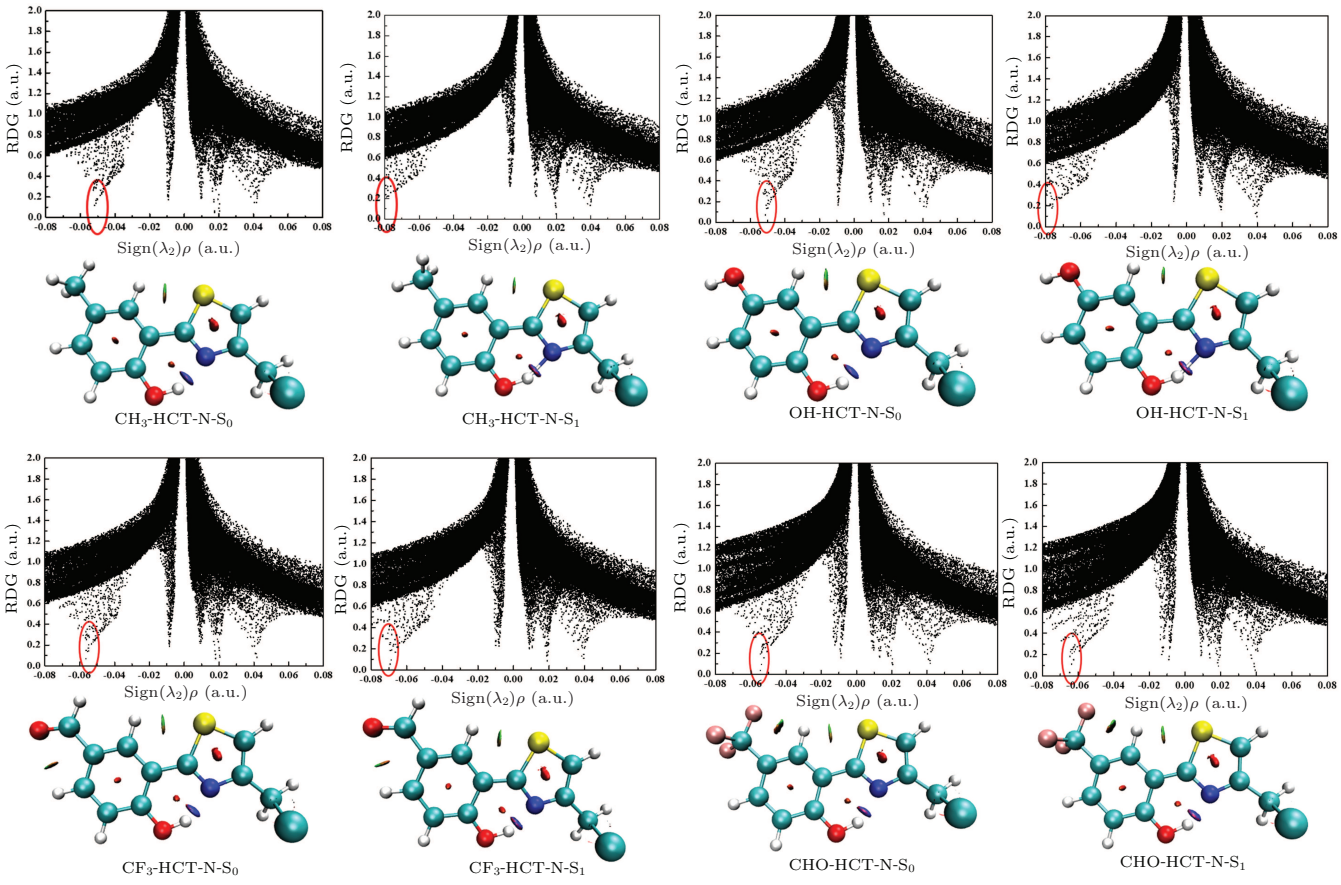


Fig. 4. Scatter plots of *S versus* sign(λ_2)ρ and gradient isosurfaces of R-HCT (R: CH_3, OH, CF_3, CHO) in S_0 state and S_1 state.

These results mean that the strong intramolecular H-bonds exist in the R-HCT (R: CH_3, OH, CF_3, CHO) in the S_0 state and S_1 state, and the H-bond in the S_1 state is stronger than that in the S_0 state. The same conclusion is obtained from the value of E_{HB} of R-HCT. Evidently, the introduction of different substituents gives rise to different effects on the H-bond strength. In the S_0 state, the electron-donating group (CH_3, OH) weakens the intramolecular H-bond of HCT, and the electron-withdrawing group (CF_3, CHO) strengthens the corresponding H-bond. In the S_1 state, the introducing electron-donating group (CH_3, OH) and electron-withdrawing group (CF_3, CHO) make the intramolecular H-bond of HCT strengthen and weaken, respectively. The above conclusion is consistent with that drawn from the structures.

We also employ the reduced density gradient (RDG) function to analyze the intramolecular H-bond of R-HCT. The RDG analysis proposed by Johnson *et al.*[53] and García *et al.*[54] is based on the electron density ρ and its reduced gradient S, and can be used to distinguish non-covalent bond interaction. Herein, a real space function $\text{sign}(\lambda_2)\rho$ is defined, in which ρ is the electron density in corresponding region and λ_2 is the second largest eigenvalue of Hessian matrix of ρ. Large negative or positive value of $\text{sign}(\lambda_2)\rho$ represents the interaction such as H-bond or steric effect, respectively. The near zero value of $\text{sign}(\lambda_2)\rho$ represents weak van der Waals interactions.

The RDG *versus* $\text{sign}(\lambda_2)\rho$ of R-HCT (R: CH_3, OH, CF_3, CHO) in the S_0 state and S_1 state are shown in Fig. 4. For the S_0 and S_1 R-HCT compounds, their spike peaks are located at $-0.06 < \rho < -0.05$ a.u. and $-0.09 < \rho < -0.06$ a.u., respectively, which confirms that the strong intramolecular H-bond O_1–H_2…N_3 exists separately in the S_0 state and S_1 state, and the intramolecular H-bonds in the S_1 state are stronger than those in the S_0 state. In comparison with HCT,[47] the introduced electron-donating/electron-withdrawing group weakens/enhances and enhances/weakens the intramolelcular H-bond of HCT in the S_0 and S_1 states, respectively. Based on the non-covalent interaction analysis, the above-mentioned conclusion is affirmed again.

3.3. Excited-state intramolecular proton transfer

In order to further study the effects of different substitutents on ESIPT process of HCT, we completely optimize the structure of transition state (TS). The TS structures of R-HCT (R: CH_3, OH, CF_3, CHO) are verified by frequency calculations as shown in Fig. A1 in Appendix A. The reaction barrier and reverse reaction barrier in the S_0 state and S_1 state of the studied compounds are calculated and displayed in Table 3. The corresponding energy diagram for proton transfer in R-HCT is shown in Fig. 5. It is worth noting that only S_1 tautomer geometries of R-HCT (R: CH_3, OH, CF_3, CHO) are obtained. All the attempts to obtain the tautomer structures of CH_3-HCT, OH-HCT, CF_3-HCT, and CHO-HCT fail and end in their corresponding normal structures. This is probably because the energy values of forming the stable tautomer structures in the S_0 state are too high.

Table 3. Calculated reaction barrier (in units kcal/mol) for forward and reverse proton transfer in R-HCT (R: CH_3, OH, CF_3, CHO) in S_1 state.

Compound	Forward	Reverse
HCT[47]	0.53	6.25
CH_3-HCT	0.20	5.62
OH-HCT	0.52	4.02
CF_3-HCT	0.96	7.54
CHO-HCT	0.58	8.11

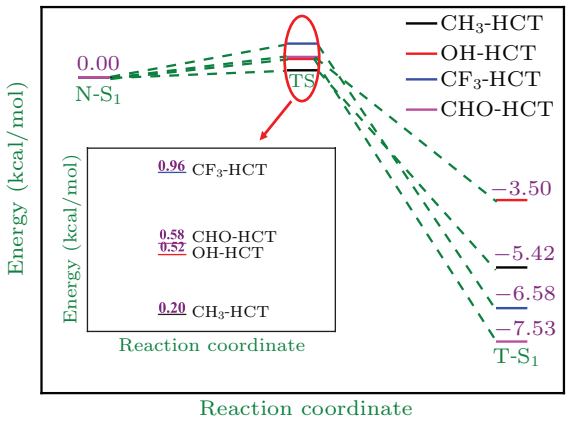


Fig. 5. Potential energy profiles of proton transfer in R-HCT (R: CH_3, OH, CF_3, CHO) in S_1 state.

These result suggest that the proton transfer from O–H group to thiazolic nitrogen atom is impossible for R-HCT (R: CH_3, OH, CF_3, CHO) in the ground state. However, it should be mentioned that there is a low reaction barrier less than 1 kcal/mol in the S_1 state for proton transfer process from N to T. Obviously, the low reaction barrier is prone to ESIPT process. The ESIPT process should be an ultrafast process due to the lower barrier. After ESIPT behavior, the S_1 tautomer form of R-HCT (R: CH_3, OH, CF_3, CHO) will transform into the corresponding unstable S_0 tautomer structure through emission fluorescence, then occur a barrierless reverse ground-state proton transfer (RGSPT) process and return to the most stable S_0 normal structure. We also find that the replacement of different substituents can modulate the ESIPT process of HCT. As shown in Table 3, the electron-donating group (CH_3, OH) and electron-withdrawing group (CF_3, CHO) reduce and increase the ESIPT reaction barrier of HCT, respectively. Evidently, the introduction of electron-donating group into the HCT is more favorable to the ESIPT process. In addition, the reverse proton transfer barrier of CH_3-HCT, OH-HCT, CF_3-HCT, and CHO-HCT are 5.62, 4.02, 7.54, and 8.11 kcal/mol, respectively, and they are all higher than the corresponding ESIPT barrier. The larger reaction barrier implies that the reverse ESIPT process is difficult to occur, and the corresponding tautomer structures of R-HCT (R: CH_3, OH, CF_3, CHO) are the stable structures in the S_1 state.

3.4. Frontier molecular orbitals and electronic spectra

As is well known, the analysis of frontier molecular orbitals (FMOs), as an effective method, is often used to explore the charge distribution characteristics in the excited state.[55,56] Therefore, the calculated FMOs of R-HCT (R: CH_3, OH, CF_3, CHO) are displayed in Fig. 6. The calculated absorption and fluorescence emission wavelengths, corresponding oscillator strength (f) and the orbital compositions are listed in Tables 4 and 5. Obviously, the first singlet transition (S_0–S_1) of R-HCT corresponds to the electronic transition from the highest occupied molecular orbital (HOMO) to the lowest unoccupied molecular orbital (LUMO), making large orbital contributions (see Table 4). Hence, only the HOMO and LUMO orbitals of R-HCT in the S_1 state are displayed in Fig. 6. From Fig. 6, we can draw the conclusion that the HOMOs of R-HCT (R: CH_3, OH, CF_3, CHO) have π character while the corresponding LUMOs have π^* character. The transition process from HOMO to LUMO has $\pi\pi^*$-type features in view of the charge distribution between HOMO and LUMO.

For the R-HCT (R: CH_3, OH, CF_3, CHO), the electron density of hydroxyl O_1 atom (proton donor) decreases, while the electron density of N_3 atom (proton acceptor) increases after the transition from HOMO to LUMO. Namely, the intramolecular charge transfer exists in the $S_0 \rightarrow S_1$ transition, and renders the hydroxyl O_1 atom and N_3 atom more acidic and basic, respectively, which is more favorable to the occurrence of ESIPT. However, the remarkable intramolecular charge transfer features in R-HCT (R: CH_3, OH, CF_3, CHO) compound are totally different because of different substituents. We find that the HOMOs of CH_3-HCT and OH-HCT are mainly located on the hydroxyl benzene ring, whereas the LUMOs are distributed mainly on phenol-thiazole ring due to push-pull electron effect (CH_3 and OH as electron donor and thiazole as electron acceptor). While for the CF_3-HCT compound and CHO-HCT compound, electron densities of both HOMOs and LUMOs are mainly in phenol-thiazole ring due to the electron-withdrawing effects of CF_3 and CHO.

Table 4. Values of vertical excitation energy of $S_0 \rightarrow S_n$ (n = 1–3) and oscillator strength (f), and major orbital contributions of R-HCT (R: H, CH_3, OH, CF_3, CHO) obtained at TD-B3PW91/6-31+G(d,p) level in acetonitrile.

	Transition	f	λ (nm)	Orbital contributions
HCT[47]	$S_0 \rightarrow S_1$	0.4976	336(325)[a]	HOMO→LUMO (97.7%)
	$S_0 \rightarrow S_2$	0.2116	289	HOMO-1→LUMO (94.9%)
	$S_0 \rightarrow S_3$	0.0503	255	HOMO→LUMO+1 (93.4%)
CH_3-HCT	$S_0 \rightarrow S_1$	0.4373	347	HOMO→LUMO (98.1%)
	$S_0 \rightarrow S_2$	0.2775	293	HOMO-1→LUMO (95.8%)
	$S_0 \rightarrow S_3$	0.0267	262	HOMO→LUMO+1 (95.0%)
OH-HCT	$S_0 \rightarrow S_1$	0.3353	373	HOMO→LUMO (98.7%)
	$S_0 \rightarrow S_2$	0.3632	296	HOMO-1→LUMO (96.4%)
	$S_0 \rightarrow S_3$	0.0068	272	HOMO→LUMO+1 (96.2%)
CF_3-HCT	$S_0 \rightarrow S_1$	0.5344	328	HOMO→LUMO (96.3%)
	$S_0 \rightarrow S_2$	0.1381	281	HOMO-1→LUMO (88.7%)
	$S_0 \rightarrow S_3$	0.0180	246	HOMO→LUMO+1 (57.7%)
CHO-HCT	$S_0 \rightarrow S_1$	0.5114	328	HOMO→LUMO (63.5%)
	$S_0 \rightarrow S_2$	0.0001	320	HOMO-2→LUMO+1(71.9%)
	$S_0 \rightarrow S_3$	0.1387	308	HOMO→LUMO+1 (54.1%)

[a]Experimental data from Ref. [33].

Table 5. Values of vertical emission energy of $S_1 \rightarrow S_0$ and oscillator strength (f), and major orbital contributions of R-HCT (R: H, CH_3, OH, CF_3, CHO) obtained at TD-B3PW91/6-31+G(d,p) level in acetonitrile.

	Form	f	λ (nm)	Orbital contributions
HCT[47]	N	0.5673	384(385)[a]	LUMO→HOMO (98.2%)
	T	0.3333	481(508)[a]	LUMO→HOMO (99.3%)
CH_3-HCT	N	0.3995	402	LUMO→HOMO (98.7%)
	T	0.3226	502	LUMO→HOMO (99.8%)
OH-HCT	N	0.3176	438	LUMO→HOMO (99.3%)
	T	0.3278	536	LUMO→HOMO (100%)
CF_3-HCT	N	0.6276	381	LUMO→HOMO (98.3%)
	T	0.3422	467	LUMO→HOMO (99.4%)
CHO-HCT	N	0.6378	379	LUMO→HOMO (94.7%)
	T	0.4459	451	LUMO→HOMO (99.5%)

[a]Experimental data from Ref. [33].

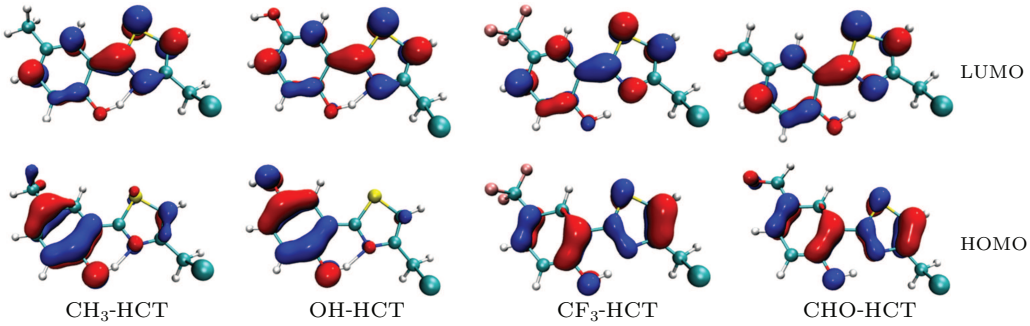


Fig. 6. Frontier molecular orbitals (HOMO and LUMO) of R-HCT (R: CH_3, OH, CF_3, CHO) in acetonitrile.

The related energy values of HOMO, LUMO, energy gap of R-HCT (R: H, CH_3, OH, CF_3, CHO) in the S_1 states are listed in Table 6. It can be seen that the HOMO and LUMO energy values of CF_3-HCT and CHO-HCT are all a little lower than those of HCT, which does not render the energy gaps of CF_3-HCT and CHO-HCT significantly different from those of HCT. For compounds with electron-donating group (CH_3, OH), the LUMO energy values are obviously increased while their LUMO energy values are a little increased, which results in the smaller energy gaps than that of HCT. The smaller en-

ergy gaps of CH_3-HCT, OH-HCT are corresponding to the red-shift absorption peaks. The smaller the energy gap, the stronger the red-shift absorption peak is.

Table 6. Energy values (in unit eV) of HOMO, LUMO, and the HOMO–LUMO gaps (in unit eV) of HCT and their derivatives R-HCT (R: CH_3, OH, CF_3, CHO) in S_1 state.

Energy (eV)	HOMO (eV)	LUMO (eV)	Gap (eV)
HCT[47]	–6.087	–2.302	3.785
CH_3-HCT	–5.909	–2.242	3.667
OH-HCT	–5.645	–2.271	3.374
CF_3-HCT	–6.295	–2.518	3.777
CHO-HCT	–6.306	–2.498	3.808

The absorption and fluorescence spectra of R-HCT (R: CH_3, OH, CF_3, CHO) at the normal and tautomer forms are also simulated and the results are shown in Fig. 7. The detailed transition properties of R-HCT (R: CH_3, OH, CF_3, CHO) are listed in Tables 4 and 5. As shown in Tables 4 and 5 and Fig. 7, it can be found that the maximum absorption peaks of CH_3-HCT, OH-HCT, CF_3-HCT, and CHO-HCT are at 347 nm, 373 nm, 328 nm, and 328 nm, respectively. And the corresponding maximum fluorescent peaks are at 402 nm, 438 nm, 381 nm, and 379 nm. The electron-donating group (CH_3, OH) gives rise to a red-shift in both the absorption and fluorescent peaks of HCT, which results in an increase in the Stokes shift (from 48 nm (HCT) to 55 nm (CH_3-HCT) and 65 nm (OH-HCT)). However, the electron-withdrawing group (CF_3, CHO) makes the electronic spectra blue-shift a little. The red-shift or blue-shift electronic spectral wavelengths imply that the intramolecular H-bond is strengthened or weakened.[57,58] Obviously, electron-donating group (CH_3, OH) and electron-withdrawing group (CF_3, CHO) strengthen and weaken the intramolecular H-bond O_1-H_2…N_3 in the S_1 state, respectively.

The calculated fluorescence spectra of R-HCT (R: CH_3, OH, CF_3, CHO) show dual fluorescent emission bands which correspond to their normal and tautomer forms, respectively. For the tautomer forms of R-HCT, the fluorescence peaks of CH_3-HCT, OH-HCT, CF_3-HCT, and CHO-HCT are at 502 nm, 536 nm, 467 nm, and 451 nm, respectively, showing the corresponding Stokes shift of 155 nm, 163 nm, 139 nm, and 123 nm. The effects of different substituents on the fluorescent emission peaks in the tautomer form are consistent with those on the absorption peaks and fluorescent peaks in the normal form.

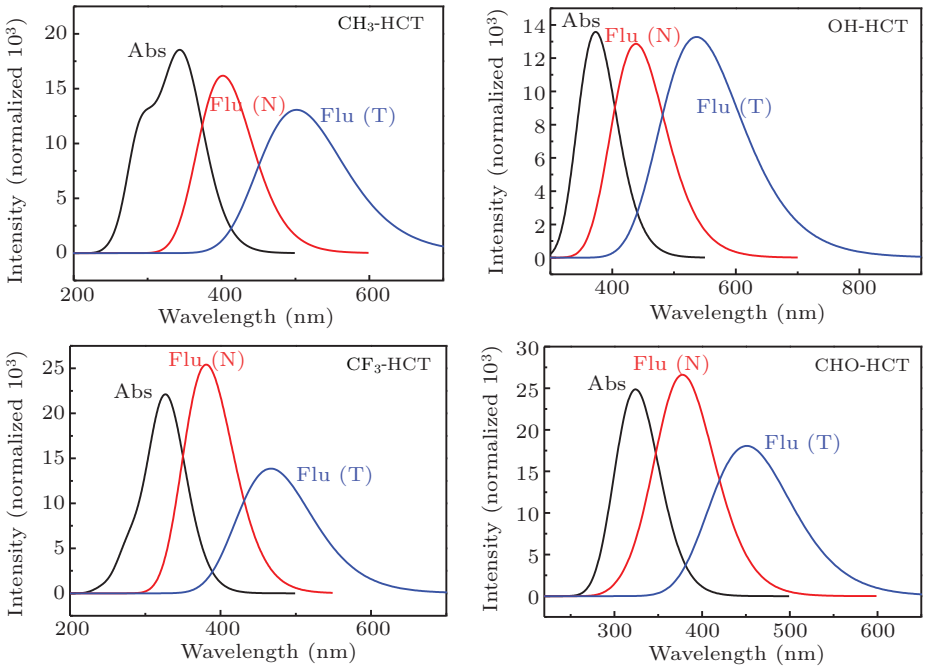


Fig. 7. Calculated absorption (Abs) and fluorescence (Flu) emission spectra of R-HCT (R: CH_3, OH, CF_3, CHO) in acetonitrile.

4. Conclusions

In summary, DFT and TD-DFT methods with IEFPCM solvent model have been used to investigate the effects of different substituents on the H-bond strength, ESIPT behaviors and photophysical properties of R-HCT (R: CH_3, OH, CF_3, CHO) compounds in acetonitrile. From the results of primary structural parameters, infrared (IR) vibration spectra, topological analysis and reduced density gradient (RDG) analysis, the strengths of intramolecular H-bond of all title compounds enhanced in the S_1 state are confirmed, which will be favorable for the ESIPT process. The electron-donating groups (CH_3, OH) and electron-withdrawing groups (CF_3, CHO) strengthen and weaken the intramolecular H-bond in the S_1 state, respectively. The enhanced intramolecular H-bond in the CH_3-HCT and OH-HCT and the weakened H-bond in the CF_3-HCT and CHO-HCT make ESIPT process take place much more eas-

ily and more difficultly, respectively. The substitution effect on the H-bond strength in the S_0 state is opposite. The frontier molecular orbitals prove that the transition process from HOMO to LUMO in R-HCT compounds show $\pi\pi^*$-type feature. The electron-donating groups (CH_3, OH) narrow the energy gaps of HCT, and electron-withdrawing groups (CF_3, CHO) do not show significant difference from those of HCT. The smaller the energy gap, the stronger the red-shift absorption peakis. In addition, the electron-donating groups (CH_3, OH) red-shift both the absorption and fluorescence emission peaks of HCT, respectively, and then causing the Stokes shift to increase. The electron-withdrawing groups (CF_3, CHO) have a little effect on electronic spectra.

Appendix A: Supporting information

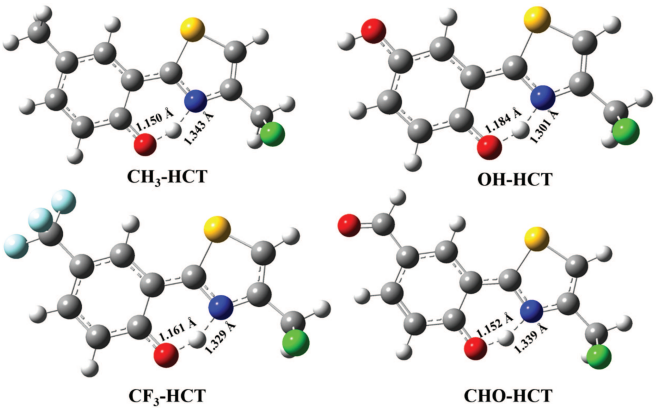


Fig. A1. Optimized transition state of R-HCT (R: CH_3, OH, CF_3, CHO) in the S_1 state.

References

[1] Horke D A, Watte H M, Smith A D, Jager E, Springate E, Alexander O, Cacho C, Chapman R T and Minns R S 2016 *Phys. Rev. Lett.* **117** 163002

[2] Dommett M, Rivera M and Crespo-Otero R 2017 *J. Phys. Chem. Lett.* **8** 6148

[3] Zhou P W and Han K L 2018 *Acc. Chem. Res.* **51** 1681

[4] Chipem F A S, Mishra A and Krishnamoorthy G 2012 *Phys. Chem. Chem. Phys.* **14** 8775

[5] Zhou H Q, Li L, Zhao Y, Wang H G and Zheng Z 2019 *Spectrochim. Acta, Part A* **208** 32

[6] Li C Z, Ma C, Li D L and Liu Y F 2016 *J. Lumin.* **172** 29

[7] Weller A 1956 *Zeitschrift für Elektrochemie* **60** 1144

[8] Peng X J, Wu Y K, Fan J L, Tian M Z and Han K L 2005 *J. Org. Chem.* **70** 10524

[9] Wu J S, Liu W M, Ge J C, Zhang H Y and Wang P F 2011 *Chem. Soc. Rev.* **40** 3483

[10] Heller A and Williams 1970 *J. Phys. Chem.* **74** 4473

[11] Parthenopoulos D A, McMorrow D P and Kasha M 1991 *J. Phys. Chem.* **95** 2668

[12] Kim J S and Quang D T 2007 *Chem. Rev.* **107** 3780

[13] Park S, Kwon J E, Kim S H, Seo J, Chung K, Park S Y, Jang D J, Medina B M, Gierschner J and Park S Y 2009 *J. Am. Chem. Soc.* **131** 14043

[14] Sedgwick A C, Dou W T, Jiao J B, Wu L, Williams G T, Jenkins A T A, Bull S D, Sessler J L, He X P and James T D 2018 *J. Am. Chem. Soc.* **140** 14267

[15] Sedgwick A C, Wu L, Han H H, Bull S D, He X P, James T D, Sessler J L, Tang B Z, Tian H and Yoon J 2018 *Chem. Soc. Rev.* **47** 8842

[16] Tang K C, Chang M J, Lin T Y, Pan H A, Fang T C, Chen K Y, Hung W Y, Hsu Y H and Chou P T 2011 *J. Am. Chem. Soc.* **133** 17738

[17] Sun C F, Li H, Yin H, Li Y Z and Shi Y 2018 *J. Mol. Liq.* **269** 650

[18] Tang Z, Wei H W and Zhou P W 2020 *J. Mol. Liq.* **301** 112415

[19] Han J H, Cao B F, Li Y, Zhou Q, Sun C F, Li B, Yin H and Shi Y 2020 *Spectrochim. Acta A* **231** 118086

[20] Yordanov D, Deneva V, Georgiev A, Crochet A, Fromm K M and Antonov L 2020 *Spectrochim. Acta Part A* **237** 118416

[21] Zhang N N, Liu D B, Chen W F, Liu X and Yan J Y 2020 *Comput. Theor. Chem.* **1185** 112898

[22] Qi Y T, Wang Y, Tang Z, Liu J Y, Hou Y M, Gao Z Q, Tian J and Fei X 2020 *J. Mol. Liq.* **314** 113614

[23] Cao B F, Han J H, Zhou Q, Sun C F, Li Y, Li B, Yin H and Shi Y 2020 *J. Mol. Liq.* **303** 112627

[24] Jia L F and Liu Y F 2020 *Spectrochim. Acta Part A* **242** 118719

[25] Yang D P, Jia M, Zhang Q L and Wang Y S 2020 *J. Lumin.* **219** 116913

[26] Watwiangham A, Roongcharoen T and Kungwan N 2020 *J. Photochem. Photobio. A* **389** 112267

[27] Ma Y Z, Yang Y F, Lan R F and Li Y Q 2017 *J. Phys. Chem. C* **121** 14779

[28] Takagi K, Yamada Y, Fukuda R, Ehara M and Takeuchi D 2018 *New J. Chem.* **42** 5923

[29] Song Y Z, Liu S S, Lu J J, Zhang H, Zhang C Z and Du J 2019 *Chin. Phys. B* **28** 093102

[30] Zhang X, Han J H, Li Y, Sun C F, Su X, Shi Y and Yin H 2020 *Chin. Phys. B* **29** 038201

[31] Zhang N N, Liu G J, Yan J Y, Zhang T T and Liu X 2020 *Dyes Pigm.* **175** 108128

[32] Kim B Y, Kim H S and Helal A 2015 *Sensors Actuat. B Chem.* **206** 430

[33] Lim C, An M, Seo H, Huh J H, Pandith A, Helal A and Kim H S 2017 *Sensors Actuat. B Chem.* **241** 789

[34] Helal A, Kim S H and Kim H S 2010 *Tetrahedron* **66** 9925

[35] Helal A, Kim S H and Kim H S 2013 *Tetrahedron* **69** 6095

[36] Helal A, Kim S B and Kim H S 2011 *Bull. Kor. Chem. Soc.* **32** 3123

[37] Seo H, An M, Kim B Y, Choi J H, Helal A and Kim H S 2017 *Tetrahedron* **73** 4684

[38] Frisch M J, Trucks G W, Schlegel H B, *et al.* Gaussian 09, Rev. D.01 (Gaussian, Inc., Wallingford, 2009)

[39] Becke A D 1988 *Phys. Rev. A* **38** 3098

[40] Stephens P J, Devlin F J, Chabalowski C F and Frisch M J 1994 *J. Phys. Chem.* **98** 11623

[41] Perdew J P 1991 *Electronic structure of solids*' 91, eds: Ziesche P and Eschrig H (Berlin: Akademie Verlag)

[42] Cancès E, Mennucci B and Tomasi J 1997 *J. Chem. Phys.* **107** 3032

[43] Cossi M, Barone V, Mennucci B and Tomasi J 1998 *Chem. Phys. Lett.* **286** 253

[44] Mennucci B and Tomasi J 1997 *J. Chem. Phys.* **106** 5151

[45] Lu T and Chen F W 2012 *J. Comput. Chem.* **33** 580

[46] Humphrey W, Dalke A and Schulten K 1996 *J. Mol. Graph. Model.* **14** 33

[47] Liang X N and Fang H 2021 *Photochem. Photobio. Sci.* **20** 533

[48] Zhao G J and Han K L 2008 *Biophys. J.* **94** 38

[49] Zhao J F, Yao H B, Liu J Y and Hoffmann M R 2015 *J. Phys. Chem. A* **119** 681

[50] Yu F B, Li P, Wang B S and Han K L 2013 *J. Am. Chem. Soc.* **135** 7674

[51] Bader R F W and Essén H 1984 *J. Chem. Phys.* **80** 1943

[52] Stasyuk A J, Cyranski M K, Gryko D T and Solà M 2015 *J. Chem. Theory Comput.* **11** 1046

[53] Johnson E R, Keinan S, Sánchez P M, GarcíaJ C, Cohen A J and Yang W 2010 *J. Am. Chem. Soc.* **132** 6498

[54] García J C, Johnson E R, Keinan S, Chaudret R, Piquemal J P, Beratan D N and Yang W T 2011 *J. Chem. Theory Comput.* **7** 625

[55] Zhao G J, Northrop B H, Han K L and Stang P J 2010 *J. Phys. Chem. A* **114** 9007

[56] Zhao X H, Liu Y F, Zhou L C, Li Y Z and Chen M D 2010 *J. Lumin.* **130** 1431

[57] Zhao G J and Han K L 2012 *Acc. Chem. Res.* **45** 404

[58] Zhao G J, Liu J Y, Zhou L C and Han K L 2007 *J. Phys. Chem. B* **111** 8940